Discover Applied Sciences

RESEARCH Open Access

Conceptualization design and analysis of lightweight composite rims for a formula student race car with a review of existing concepts

Kevin Klemt[1,3], Raffael Bogenfeld[1*†], Jean Lefèvre[1†] and Louisa Türke[2†]

Abstract

This article presents a structured design process for lightweight carbon fiber rims tailored to an electric Formula Student race car. Unlike prior work that focuses mainly on geometry or material selection, the contribution here is an integrated design approach that enables geometry-invariant laminate sizing and is grounded in a structured review of existing CFRP rim and wheel concepts. The process includes the concept development, structural finite element analysis, and the integration of manufacturing considerations within a framework tailored to the resource and time constraints typical of Formula Student projects. This review clarifies typical mass savings, concept choices, and validation strategies and provides the reference frame for the subsequent design. Drawing on this review, three design solutions were evaluated: a composite rim with an aluminum center disk, a full composite spoke rim, and a full composite flange rim. Considering the integration with the existing vehicle architecture and manufacturing feasibility, the hybrid rim with a metallic center disk was selected. A suitable laminate design was achieved iteratively via finite element simulations to meet strength and stiffness requirements. The final configuration, a symmetric stacking sequence with alternating 0° and 45° plies of woven carbon fiber fabric, is governed by the displacement limits under the cornering load case. Safety margins against strength and fatigue failure were confirmed for all relevant Formula Student load cases. Eventually, manufacturability aspects were incorporated in an enhanced numerical simulation that reflects realistic ply draping and supports the preparation of tooling and layup definition. The developed rim satisfies the camber-angle stiffness requirement and maintains safety factors of approximately 1.5 in compression and 1.8 in tension and achieves weight savings of 49 % compared to an aluminum reference. This reduction approximately halves the rim's polar mass moment of inertia and, together with the 3% vehicle mass reduction, is expected to improve acceleration, braking response, and ride quality for the Formula Student car. Still, the main contribution of this article lies in a transferable methodology for CFRP rim design that combines the laminate design process with realistic manufacturing and vehicle integration constraints and is informed by the synthesized literature on composite rims for Formula Student and automotive applications.

†Raffael Bogenfeld, Jean Lefèvre and Louisa Türke have contributed equally to this work.

This article presents a structured design process for lightweight carbon fiber rims tailored to an electric Formula Student race car.

*Correspondence:
Raffael Bogenfeld
raffael.bogenfeld@dlr.de
[1]Institute of Lightweight Systems, German Aerospace Center, Lilienthalplatz 7, 38108 Braunschweig, Germany
[2]Institute for Engineering Design, Technische Universität Braunschweig, Hermann-Blenk-Str. 42, 10587 Braunschweig, Germany
[3]Lions Racing Team e.V., Hermann-Blenk-Str. 42, 38108 Braunschweig, Germany

Keywords Composite rims, Race car, Review, Finite element analysis, Lightweight structures, Formula student

Graphical abstract

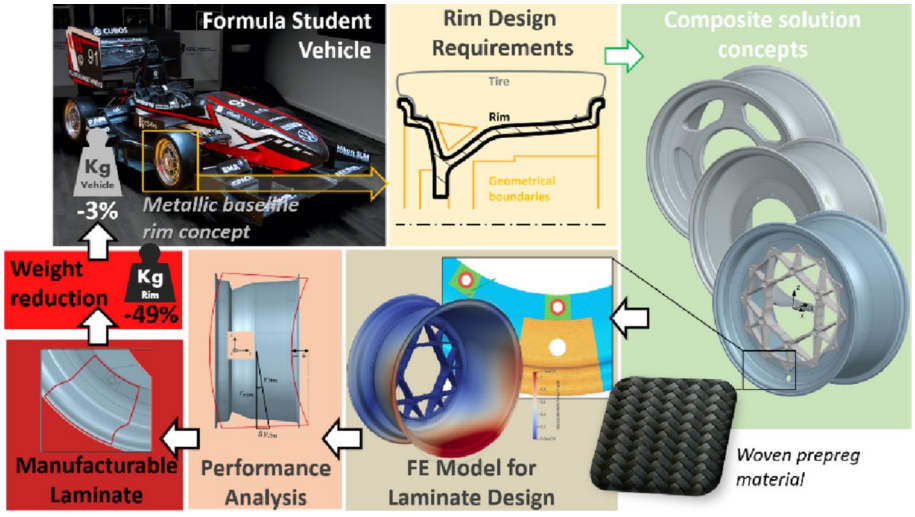

1 Introduction

The Formula Student (FS) is a globally recognized engineering competition in which student teams from different universities develop, build, and race their own formula-style vehicles (see Fig. 1). The competition is governed by a comprehensive set of rules that are updated annually, for instance by the Formula Student Germany [1], covering technical requirements, safety protocols, administrative procedures, and event formats. Since its initiation in 1981 by the Society of Automotive Engineers (SAE), the FS and its rules have significantly evolved over the decades to reflect technological advances [2]. A particular class for alternatively-fueled vehicles was introduced in 2008, opening the competition for electrical race cars. In 2025, 84 registered teams participated in the competition of the [3].

In this competitive environment, every component of the vehicle is scrutinized for performance, efficiency and innovation. Nonetheless, the development cycles are short: for example Mihailidis et al. [4] documented completing the development of an entire Formula Student vehicle in just nine months. Hence, the progression is often incremental and newly developed components are frequently integrated in prototype form without full validation.

Lightweight structural design is a central topic in modern automotive engineering, driven by regulatory pressure, efficiency targets, or performance requirements. Recent reviews highlight the growing role of composites and hybrid material systems, as well as advanced manufacturing routes, in achieving substantial mass savings while maintaining structural performance [5, 6]. According to the state-of-the-art, structural optimization methods are increasingly applied at component and vehicle level [7–9], for example in composite body structures and floors, where multidisciplinary optimization yields significant weight reductions under stiffness and strength constraints [6]. Multi-material

Fig. 1 Formula Student race car of the Lions Racing Team from the Technische Universität (TU) Braunschweig

design frameworks further integrate lightweight and cost in an early conceptual design stage [10]. Moreover, the crashworthiness of composite automotive structures is a key feature which can reliably be demonstrated through finite element models, supporting the use of composites in safety-relevant parts [11]. Against this background, lightweight composite rims for Formula Student can be viewed as a specific application of these general trends in automotive lightweight and structural optimization.

Nonetheless, the wheel plays a critical role among the vehicle components, because it directly affects both the vehicle's dynamic behavior and its performance. Reducing the weight of the unsprung masses — such as wheels, hubs, in-wheel motors, and brake systems — can significantly improve the handling, braking, and acceleration of a vehicle as outlined by Hrovat [12].

A lighter rim not only reduces the rotational inertia, but it also lowers the overall energy demand and steering forces during dynamic maneuvers. These benefits have also been recognized in the FS community, with several teams documenting their developments in technical reports and scientific publications, for instance Walther [13], Sorrenti and Smout [14], or Bhagwat [15].

In FS cars with electric in-wheel motors, the mass of the drive unit increases the unsprung mass Ślaski et al. [16] and, thus, the dynamic loads Wu et al. [17], which further enhances the need for lightweight wheels. To counter these unwanted effects, ambitions to reduce the unsprung mass of in-wheel motors have been made, for example by Luo and Tan [18]. Given these factors, the development of a lightweight wheels made from fiber-reinforced plastics emerges as a promising solution for achieving high performance through incorporation of a novel technology.

Formula Student vehicles are equipped with either 13-inch or 10-inch wheels. While 13-inch rims were traditionally favored due to tire availability cf. [19] and provide more space for components inside the wheel, as outlined by Sorrenti and Smout [14]. However, Orlando [20], who describes the transition from 13" to 10" rims, outlines that 10" rims offer a reduced unsprung mass and rotational inertia, enhanced handling and efficiency. The smaller diameter also facilitates lighter suspension components but constrains brake size and ground clearance. The optimal rim size depends on the team's design priorities which include the vehicle dynamics, integration constraints, and component availability.

Many teams adopt readily available off-the-shelf wheels before own designs are finished [21–23]. Such commercial rims for FS cars are for example supplied by Keizer Wheels in the US [24] or OZ Racing from Italy [25]. The reported masses of Keizer rims

ranges from 2 kg to 3.5 kg according to Rohan [26]. The individual rim choice depends on the particular vehicle specifications. For example, Walther [13] and Aggarwal and Elsen [27] use a 13 inch rim 3.5 kg as a reference configuration while Korntved et al. [21] consider a 10 inch Keizer wheel with a weight of 1.85 kg. These values provide a baseline to assess individual CFRP rim designs.

Rims made from carbon fiber reinforced plastics (CFRP) offer significant weight savings and performance advantages over conventional metallic rims as Czypionka and Kienhöfer [28] describe. Also Kandukuri et al. [29] explain how utilizing carbon fiber wheels reduces the overall vehicle mass, resulting in better handling characteristics for the race car. A number of FS teams and researchers have explored the potential of CFRP rims. A brief review of publications about CFRP rim designs in the FS from the literature summarizes the common design approaches and enables a quantification of the potential weight benefits.

The overview Fig. 2 illustrates the total rim mass and the corresponding weight reduction reported in various studies on CFRP rims for FS vehicles. The majority of published work has focused on 10" rims, whereas only a few studies address 13" configurations. Reported weight savings range between 30 % and 60 % compared to aluminum reference rims. Even though 10" rims are generally lighter than their 13" counterparts, the relative weight benefit of CFRP is comparable for both wheel sizes.

The reviewed concepts in Fig. 2 can be categorized into full composite and hybrid rims. Full composite designs have been developed by Walther [13], Bol'shikh et al. [23], Korntved et al. [21], Bhagwat [15], Kandukuri et al. [29], Unti et al. [30], and Uyttersprot [31]. In contrast, hybrid rims combine a CFRP rim with a metallic center disk. Hybrid solutions were published by Walther [13], Unti et al. [30], Uyttersprot [31], and Bhagwat [15]. In addition, Aggarwal and Elsen [27] propose an unconventional hybrid where a composite center disk is mounted to an aluminum rim. Comparing both categories, the diagram in Fig. 2 demonstrates that, independent of the wheel size, full composite rims are generally lighter than hybrids. This is particularly notable in studies investigating

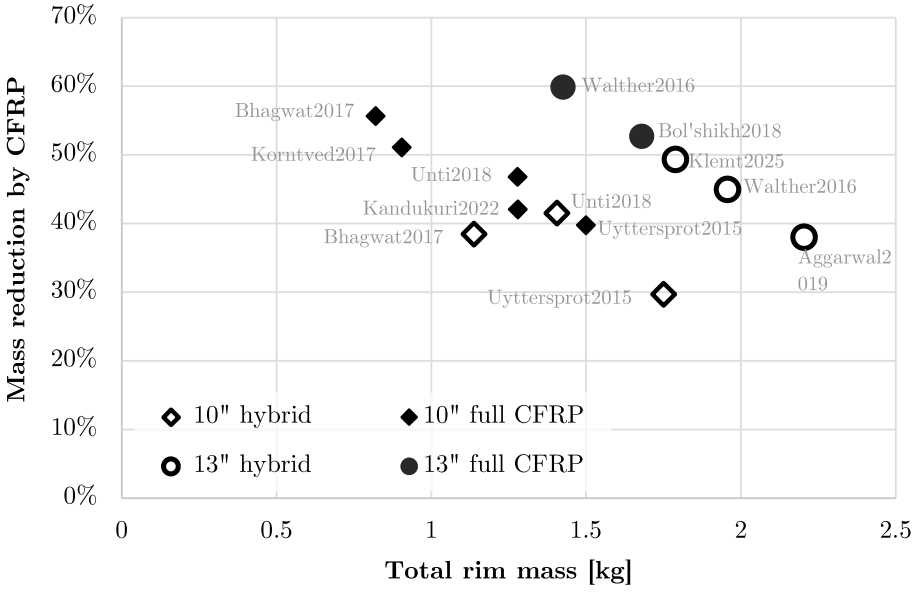

Fig. 2 Overview diagram of CFRP rim masses and mass reduction compared to aluminum rims as reported in the literature

both concepts (Walther, Unti, and Uyttersprot), where the full composite solution consistently offered a better weight benefit. Nonetheless, hybrid rims have their advantages as they are easier to manufacture and often better integrate with the wheel hub.

Table 1 summarizes CFRP rim and wheel studies from the literature, including both the works already evaluated quantitatively in Fig. 2 and additional relevant works. The studies are grouped into Formula Student/FSAE applications and other automotive wheels. The main objectives, rim concepts, and key findings are listed for each work. This overview provides a structured basis for comparing typical design approaches and validation strategies. Moreover, it helps to position the present study while highlighting the need for a transparent, transferable design methodology for CFRP rims in the Formula Student context.

Design criteria for FS rims differ substantially from those for street-legal vehicles. In the controlled race environment, accidental damage events are uncommon and the overall mileage of an FS car rarely exceeds a few hundred kilometers. Consequently, long-term durability and damage tolerance play a less dominant role in the design process and are both not directly reflected in the competition rules of the [1]. Instead, lightweight design and performance under predefined acceleration and cornering load cases are the primary objective.

By contrast, rims for street-legal vehicles must satisfy comprehensive safety and durability requirements as defined in established international standards like the ISO 14400 [43] and the ISO 3006 [44]. These standards, which are presented in this study as context only, impose structural integrity requirements under fatigue, impact, and environmental loads. Elaborate testing and validation shall ensure the reliability throughout the service life that typically range from $150,000\,\mathrm{km}$ to $300,000\,\mathrm{km}$ according to Weymar and Finkbeiner [45]. Recent studies, for example by Zanchini et al. [39], demonstrate that composite rims can be designed to meet such requirements. But this often involves additional safety margins and validation testing. Nonlinear FE analysis combined with data-driven surrogates, such as artificial neural networks, has been proposed to evaluate impact energy absorption and injury-related responses efficiently [46].

Recent work on composite rims for road vehicles therefore combines structural optimization with extensive fatigue and impact testing, including standardized 13° impact and small-overlap crash scenarios [39–41], which goes beyond what is typically feasible in an FS project.

This contrast highlights the fundamentally different priorities: Road-worthy rims must prioritize safety and durability under highly variable operating conditions. Elaborate test efforts according to standardized procedures are mandatory and scheduled within the development cycle. FS rims are designed for short service life, maximum performance, and technology demonstration. All this must be achieved within short development cycles.

Thus, developing lightweight CFRP rims from an aluminum baseline represents a significant step for a FS team. It must be approached with clear and elementary design methods. The performance requirements must be satisfied, including sufficient stiffness and adequate strength to withstand critical load cases. The rim design must also ensure compatibility with the existing wheel hub interface and respect the practical limitations of manufacturing within a student team environment. Balancing these constraints

Table 1 Summary of published CFRP rim studies for FS vehicles and related automotive wheels.

Study	Objective and rim concepts	Key findings and remarks
Formula Student: comparative composite rim studies		
Walther [13]	13" full-composite spoke rim and hybrid rim with aluminum centre disk	Demonstrates feasibility of CFRP rims in FS; full-composite spoke rim achieves $\approx 60\%$ mass reduction; hybrid concept simplifies hub integration and manufacturing
Uyttersprot [31]	Two-piece hybrid rim and one-piece full composite rim	Reports 30–40% weight reduction vs. aluminum; highlights bonding and assembly challenges; FE to assess rim flange stresses
Kandukuri et al. [29]	Composite spoke rim vs. aluminum, magnesium, titanium wheels	Reports 47% mass reduction for CFRP version; indicates further stiffness gains possible through refined ply orientation
Korntved et al. [21]	13" two-part composite rim versus aluminum reference	Achieves $51\,\%$ weight reduction with CFRP; static FE confirms structural performance; stresses importance of symmetric lay-up for stiffness
Bol'shikh et al. [23]	Two-part CFRP rim compared with magnesium wheel	Obtains $33\,\%$ mass saving vs. magnesium at comparable strength; discusses limits of simple analytical stress models for composite rims
Shekhar et al. [32]	One-piece CFRP rim benchmarked against aluminum and magnesium	Finds 40–50% weight reduction; FE analysis to verify static performance; considers manufacturing constraints
Unti et al. [30]	Hybrid rim with metallic centre disk and full-composite spoke rim	Hybrid achieves $\approx 46\%$ mass reduction; full composite reaches $\approx 59\,\%$; compares lightweight potential and manufacturability for FS use
Formula Student: composite rim design studies		
Aggarwal and Elsen [27]	Hybrid with composite center disk and aluminum rim	Proposes unconventional hybrid layout; shows potential stiffness benefits but increased complexity of the disk–rim interface
Barsony et al. [33]	Iterative FS composite rim design using manual lay-up refinement	Derives loads from lap-time simulation and experience; 11 FE-based lay-up iterations yield 35% mass reduction vs. aluminum and 15% vs. previous CFRP rim without safety loss
Ressa [34]	Woven CFRP rim for FS car to reduce mass/ inertia	Uses tests to calibrate FE simulation, then evaluates several layups; final design cuts wheel mass by nearly 50%; prototype produced for later vehicle testing
Kruse [35]	CFRP rims designed for measured suspension loads	In-service load data to size CFRP wheel; emphasizes benefits of reduced unsprung and rotating mass for handling and grip while maintaining strength
Pizot [36]	CFRP rims with aluminum centers for FS	Design and manufacturing of CFRP rims and tooling. Shift from RTM manufacturing to prepreg-compatible mold design, highlighting practical constraints in student projects
Other automotive composite rim studies		
Nishi [37]	Local CFRP reinforcement of aluminum production wheel	Applies bonded CFRP patches to tailor stiffness and reduce mass by $\approx 600\mathrm{g}$ per wheel; also enables tuning of natural frequencies for improved vibration behaviour
Malewadkar et al. [38]	FEA study of aluminum vs. optimised composite rim	Shows notable mass reduction for composite rim with acceptable stress and modal response; observes slightly higher peak deformation and higher material and manufacturing costs
Zanchini et al. [39]	Composite and aluminum spoke wheels for sports car	Composite rims reduce mass and increases bending stiffness; fatigue testsand FE analysis confirm compliance with safety targets
Wang et al. [40]	Multi-objective integrated optimisation of a carbon/aluminum hybrid rim	Surrogate model to optimise layup and thickness; achieve 17.2% weight saving against magnesium rim while meeting fatigue and impact requirements
Hwang [41]	18" hybrid wheel with CFRP rim + aluminum center disk; 13° impact studied with explicit FE	Disk remains safe in 13° impact; damage localized in rim. Damage volume used as indicator; fiber angles $> [\pm 30°]$ predicted to pass test, validated with experiments
Bisht [42]	Comparative study of 14" a Al6061 rim and a composite rim	FE analysis to model and analyse aluminum and CFRP rims under identical loads; evaluates $[\pm 35\,°]$, [± 45°], [± 55°], [± 75°] lay-ups to compare strength and weight reduction potential

defines the essential design challenge in adapting CFRP rims for Formula Student applications.

This article focuses on the development process of a CFRP rim. Based on the literature review, various solution concepts are developed and evaluated. The aim of this work is not to propose a single optimal rim geometry or a new numerical optimization algorithm, but to develop and demonstrate a transferable design methodology for composite rims in the FS context. The central contribution is a workflow that enables a geometry-invariant sizing of the laminate thickness based on an Finite Element (FE) simulation. This methodology is applied for a hybrid CFRP rim with an aluminum center disk for an FS race car, but is intended to be reusable for future rim designs and similar lightweight composite components.

The body of this article is structured as follows: Section 2 defines the functional requirements, geometric constraints, material choice, the considered rim concepts, and formulates the design objectives, variables, and constraints. Section 3 describes the numerical analysis methodology, including the load cases, FE model, and evaluation metrics. Section 4 presents the iterative laminate sizing process, the structural response under all load cases, and an enhanced validation model considering manufacturing constraints.

2 Design requirements and concept development

2.1 Functional requirements

The design of the CFRP rim is driven by functional requirements defining how the rim must transmit loads between tire and hub, maintain wheel alignment and sealing, and remain compatible with the existing suspension and brake layout. In this subsection, the key functional demands that govern the subsequent geometric design and laminate sizing are presented.

The design process of the composite rim begins with the generation of possible concepts and their systematic technical evaluation. This evaluation necessitates detailing essential requirements and constraints that the rim must satisfy. In this requirement analysis, the roles of the relevant components and features have to be considered. The corresponding definitions used in this article correspond to the standard [47] and are explained in Fig. 14 in the Appendix) The main function of the rim is to transfer forces from the tire to the wheel hub, and thereby transmitting them into the vehicle. These loads involve the moments generated during acceleration and braking maneuvers which must be effectively transmitted from the drive shaft to the road. Additionally, lateral forces during cornering must be sustained while maintaining performance, with a maximum allowable camber loss of $0.2°$ per g of lateral acceleration (performance requirement imposed by the vehicle dynamics group of the Lions Racing Team). In addition, vertical loads from the vehicle weight must be sustained without compromising stiffness.

Effective force transmission is only possible if the rim is securely connected to the wheel hub. Therefore, the wheel hub interface of the rim is a critical feature. In addition to the force transmission during operation, the rim interface must ensure the circular runout of the wheel. For this purpose, the hub interface of the rim must allow the centering relative to the wheel hub. With regard to the incremental nature of FS development, the rim design for the present study must be compatible with the existing vehicle and its wheel hub interface used for the metallic rim. Hence, a hybrid rim with a center disk has

to feature the appropriate interface for the existing disk while a one-piece full composite rim must directly fit the existing wheel hub.

The tired-sided interface of the rim must ensure a secure tire seating without slip or air pressure loss. As a result, the bead seat surface must be of high quality which is achievable either through machining or a two-sided manufacturing tooling. The sealing functionality must be guaranteed for any applicable load and temperature conditions. For instance, a temperature of $80°C$ has to be considered to account for the heat from the disk brakes inside the wheel. The allowable pressure loss for the Formula Student is limited to $0.023\,\mathrm{MPa}$ per $100\,\mathrm{km}$. Tire deflation during a competition immediately disqualifies the a team from the FSG [1]. In addition, the tire mounting and inflation procedures must be possible without causing damage to the rim.

Finally, the manufacturing feasibility and material resources must be considered, as these vary between different FS teams. For the Lions Racing Team, the rim must be manufacturable from prepreg material through hand layup with reasonable effort and an autoclave curing process.

2.2 Geometrical constraints

The rim design is governed by strict geometrical constraints arising from the specified dimensions of the by Continental C19 205/470 R13 tire, the existing wheel hub and brake layout, and the FS regulations on clearances and wheel offset. This subsection summarizes the key geometric boundaries that must be satisfied to ensure the integration of new rim with the existing vehicle.

The geometrical rim design is governed by boundary conditions that ensure compatibility with the existing tire and hub specifications. Figure 3 illustrates the respective boundaries for a hybrid rim with a center disk (Fig. 3a) and for a one-piece full composite rim (Fig. 3b). Primarily, the tire dimensions determine the required outer rim contour including key parameters such as the bead seat diameter and overall width. The rim to be designed must accommodate a C16 competition tire manufactured by Continental particularly for the FS and used, for example by Unti et al. [30]. The tire features a 205/470 R13 specification which imposes a $205\,\mathrm{mm}$ width requirement and a 13" diameter to the rim design. To enable the tire mounting, a drop center with sufficient free space is required.

On the inner side, the in-wheel components and the hub interface geometrically constrain the rim design. The rim must include space for essential components such as the brake system, suspension, and in-wheel motors. A minimum clearance of $5\,\mathrm{mm}$ between

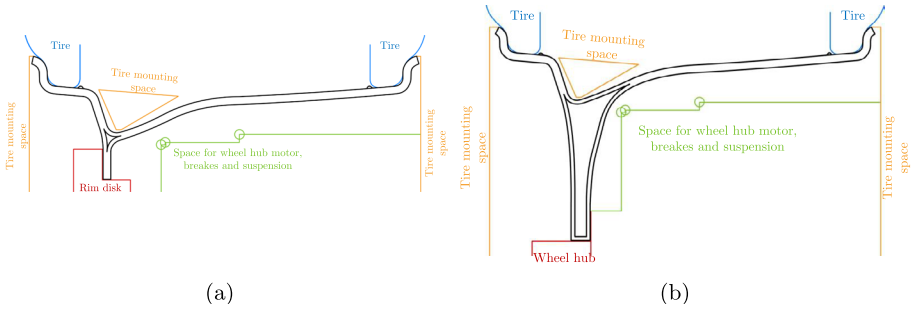

Fig. 3 Geometric boundary conditions for a hybrid composite rim with a center disk (**a**) and for one-piece full composite rim (**b**)

the rim and these components is demanded by the rules of the FSG [1]. This clearance directly imposes a requirement to the rim offset of the vehicle of Lions Racing Team. The offset of the newly developed rim must remain identical to that of the previous aluminum rim and is fixed to $48\,\mathrm{mm}$ to maintain the overall balance and clearance of the wheel assembly.

With regard to the centric interface, the hybrid rim must feature the interface to the center disk, a one-piece rim must integrate the wheel hub interface. Both variants have to ensure the wheel centering, necessitating precise dimensions for the bolt circle in case of screw centering (4a), or a the rim centering area for hub centering (4b).

Inherent to the design, the hybrid rim features a small central cavity which can be filled through a fillet manufactured from rolled unidirectional material as done by Ekermann and Hallström [48], Bogenfeld et al. [49] or even a manufactured fillet stacking, demonstrated also by Ekermann and Hallström [48]. In contrast, the one-piece rim exhibits a larger cavity, typically located within spokes, which has to be filled by a foam core.

Altogether, these geometric and functional requirements ensure that the composite rim integrates seamlessly with the vehicle's overall design while maintaining its serviceability.

2.3 Material consideration

The choice of a composite material with a carbon fiber reinforcement was driven by the outstanding strength-to-weight and stiffness-to-weight ratios and the corresponding potential for significant weight savings. With regard to the geometric complexity of the rim profile, it is essential that the composite layers have a good drapability. Woven composites are particularly advantageous in this regard. In addition, woven layers offer approximately similarly high strength and stiffness in two perpendicular directions. Consequently, laminates can be efficiently constructed using fiber orientations of $0°$ and $45°$. Among the available options, plain, twill, and satin weaves were considered; however, only twill and satin weaves provide sufficient drapability for the intricate rim geometry Mohammed et al. [50]. Based on these considerations, Cycom® 985 prepreg material was selected for the rim. The material properties required for simulation are provided in Table 4, as specified in the technical data sheet from the manufacturer, Solvay [51].

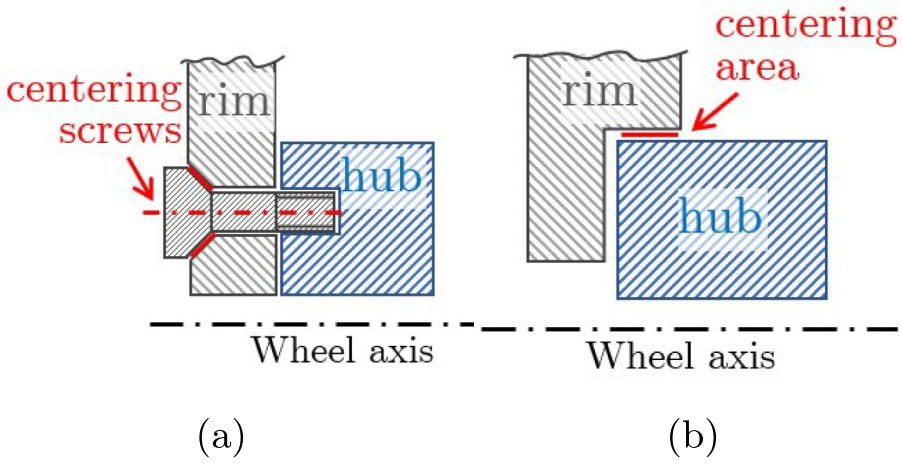

Fig. 4 Rim centering through centering screws (**a**) or a hub centering area at the rim interface (**b**).

2.4 Three solution concepts

After multiple stages of evaluation and refinement, several concepts were generated to meet the requirements. All concepts have in common that the laminate thickness must be varied inward, so that tire fit and bead geometry remain unchanged across all design concepts and laminate variants. The external load introduction as resultant forces is concept-independent and acts in the contact region between tire and rim.

Potential solutions were create in the early design phase, where initial sketches and preliminary CAD models were developed. These early models were then assessed against a set of criteria including manufacturability, applicability, and the compliance with FS standards. For example, any solution with a flat base profile was excluded since these require a multi-piece rim design. Finally, three possible solution concepts were identified for the composite rim of the vehicle of the Lions Racing Team.

2.4.1 Hybrid rim

The hybrid rim concept depicted in Fig. 5ais a straightforward design solution where the new development is limited to the rim itself, excluding the center disk, which reduces the design and the manufacturing effort. The composite rim part is coupled with an existing aluminum center disk using a screw connection with spacer elements to reduce contact pressure. The rim centering is through a centering surface between the rim and the center disk. The rim features a drop base profile and a machined bead seat area to ensure a secure pressure seal. The cavity at the drop base is expected to be small for this design variant and can, thus, be filled by rolled unidirectional material (compare with Fig. 3a). To prevent corrosion of the aluminum center disk, a protective coating on the aluminum is recommended.

2.4.2 One-piece spoke rim (full composite)

A spoke rim as shown in Fig. 5 brepresents a one-piece full composite rim concept with significant potential for a lightweight design as identified in the review section. This design employs a central hub approach for rim mounting, combining both centering and fastening functions. Due to the complex geometry of the spokes and the size of the inner cavities, foam cores are required to fill the hollow sections (compare with Fig. 3b). Furthermore, the complex spoke geometry demands a multi-piece tooling, a demanding laminate design, and a challenging manufacturing process. However, the multi-piece tooling concept would facilitate using an external tooling which directly provides a high-quality bead seat surface.

(a) Hybrid rim with center disk (b) Spoke rim (full composite) (c) Flat flange rim (full composite)

Fig. 5 Three rims concepts derived through a morphological analysis process

2.4.3 One-piece flange rim (full composite)

The flange rim in Fig. 5 crepresents another one-piece full composite rim concept. The simpler geometry in comparison to the spoke rim allows for a two-piece tooling and easier manufacturing, while the full composite design could still offer a higher lightweight potential than the hybrid rim. In contrast to the hybrid rim, the flange rim is directly attached to the wheel hub. Due to a smaller bolt circle, the transmitted moments impose higher forces to the fastening screws, making the interface design more difficult. Additional measures to improve load transfer and to reduce surface pressure might be necessary. The cavity in the drop base is larger than in a hybrid Rim but smaller than in the spoke rim, allowing for a potential forged-carbon solution or a foam core. The rim can be centered via hub centering. A high quality surface at the bead seat needs to be achieved by machining.

2.4.4 Design choice

All three concepts were developed into detailed CAD models as depicted in Fig. 5. The CAD design was created to ensure the compatibility with the existing tire and the hub design of the vehicle in Fig. 1. According to the initial literature review, the spoke rim concept offers the highest lightweight potential. However, the main drawback of the spoke rim variant is its complexity. The spokes would require a complex laminate design, a multi-part tool, and a difficult manufacturing process. All this poses a significant risk to the success of the wheel development. For these reasons, the spoke rim concept cannot be further developed within the scope of this work. Still, it remains relevant for future developments.

The flange rim is a compromise between a lightweight full composite solution and a simple-to-manufacture design. Nevertheless, this concept is rarely implemented and the literature does not provide sufficient data to quantify the its weight reduction potential. The flange rim (and also the spoke rim) faces and additional challenge regarding the hub interface. The current wheel hub leverages a form fit solution with the aluminum center disk as shown in Fig. 6. This form fit imposes practical constraints to the rim design: the CFRP rim–aluminum disk interface is a critical design challenge not only to the rim but also to the fasteners used at the wheel hub interface. Those are not suitable to sustain the wheel moments without a for fit connection. However, the realization of this interface in a composite rim is considered very challenging. Hence, any full composite rim would likely necessitate the redesign of the existing wheel hub. As this opposes the compatibility with the existing hub, only a hybrid rim design fulfills the current requirements of the Lions Racing Team.

The hybrid rim thus provides the best balance between lightweight potential, manufacturability, and vehicle integration. As a consequence, the development continues with

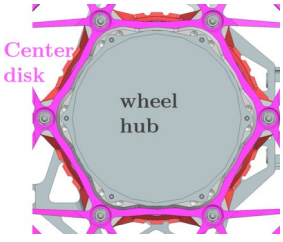

Fig. 6 Existing solution form fit solution for the interface between the wheel hub and the rim center disk

the numerical analysis and the laminate design for the hybrid rim. The reference aluminum rim used in this study is the team's current production wheel, which already satisfies all Formula Student regulations and vehicle-dynamics requirements.

2.5 Design objectives, variables, and constraints

As a next step, the laminate design for the chosen hybrid composite rim must be defined. Although mass reduction is the primary motivation for using composite rims, the laminate design objectives arise from the functional and integration requirements given in Sections 2.1 and 2.2. In addition to selecting the hybrid concept with an aluminum center disk rather than full-composite alternatives, the design variables are the laminate thickness and stacking sequence, as well as local geometric details that remain compatible with the fixed outer contour dictated by the tire. The design is constrained by a performance (stiffness) requirement, strength limits expressed through maximum stresses and safety factors under all relevant load cases, manufacturability constraints associated with prepreg processing in a two-piece tool (including feasible ply segmentation and draping), and compatibility with the existing wheel hub interface, bolt pattern, and Formula Student regulations.

Table 2 summarizes the main objectives, design variables, and constraints for the hybrid CFRP rim. To determine the laminate stacking (ply count and orientation) within this design space, the rim is analyzed using a finite element model for structural simulation.

3 Numerical analysis methodology and load case definition

A Finite Element Analysis was set up to derive a laminate design and to evaluate the structural performance of the rim.

The critical load cases were identified, a surface model of the rim was created, and necessary assumptions and idealizations regarding load introduction were applied. This simulation model enables both, a strength evaluation to prevent structural failure and a performance quantification through the camber angle loss. The numerical analysis in present FE study is restricted to quasi-static operating conditions. Dynamic excitation, detailed fatigue loading, or impact scenarios are not modeled in this work and are discussed as limitations in Discussion Section.

Table 2 Design objectives, variables, and constraints for the hybrid CFRP rim laminate sizing

Category	Item	Description/target
Objective	Rim mass	Minimize mass of CFRP rim plus aluminum center disk
Objective	Stiffness	Limit deformation to fulfill performance requirement under competition load cases
Constraint	Strength	Ply stresses within allowables (material strengths with safety factors) for all relevant load cases
Constraint	Geometry/integration	Outer contour fixed by tire; interfaces compatible with existing hub and center disk
Constraint	Manufacturability	Prepreg layup in two-piece tooling; use of woven CFRP with $0°/45°$ plies; symmetric stacking and feasible draping
Design variable	Ply count	Discrete number of CFRP plies in the rim cross section
Design variable	Ply orientation	Assignment of each ply to $0°$ or $45°$; symmetric layup about the mid-plane
Design variable	Ply grouping	Distribution of plies between rim regions (bead, drop center, flange) within the above constraints

3.1 Load cases

Functionally, the rim must withstand a variety of loads typical in racing scenarios, including static vehicle weight, cornering, braking, acceleration, and the tire inflation pressure. The applicable loading scenarios can be derived from the FSG regulations [1]. The primary goal of the analysis is to efficiently develop a safe laminate design. The final rim design must ensure sufficient structural stiffness and strength in six relevant scenarios listed below. For all operation load cases (except case 4), tire mounting, the design tire inflation pressure $p_{tire} = 0.08\,\mathrm{MPa}$ has to be considered.

The vehicle forces for each load case are resolved into three components in vehicle coordinates (visible in Fig. 5a), where F_x-, F_y-, and F_z, correspond to longitudinal, lateral and vertical forces, respectively. Aggarwal and Elsen [27] detail how the individual forces are introduced to the rim. With fixed boundary conditions at the wheel hub interface, the vehicle forces can be applied to the rim bead while the tire inflation pressure acts on the rim's outer surface. The load introduction in this work is further discussed in the model building section. For comparison, discrete loads for individual loading scenarios are given, for example, by Aggarwal and Elsen [27], by Sorrenti and Smout [14] and others [26, 29, 34].

- **Load case 1A: cornering (Formula Student maximum speed)** For a maximum curve radius of $25\,\mathrm{m}$, the tire and rim experience high lateral forces at the outer tire. The maximum reachable velocity of the Lions race vehicle in this turn is $v_{1A} = 23.13\,\mathrm{ms}^{-1}$. This case defines the critical vertical force $F_{z1A} = 1638\,\mathrm{N}$ and lateral force $F_{y1A} = 2229\,\mathrm{N}$ under competitive conditions. The crucial performance requirement to the maximum camber angle loss must be fulfilled for this load case.
- **Load case 1B: cornering (maximum vehicle speed)** At maximum vehicle speed $v_{max} = 36.1\,\mathrm{ms}^{-1}$ a larger curve radius of $41.5\,\mathrm{m}$ can be driven. This case represents the maximum tire load during curve driving at the vehicle's top speed. This condition can not occur during the race, thus the performance requirement does not apply. Nonetheless, the rim's strength must be verified under this limit condition. The respective forces are $F_{z1B} = 2361\,\mathrm{N}$ vertically and $F_{y1B} = 3027\,\mathrm{N}$ laterally.
- **Load case 2: full braking** This case simulates the peak longitudinal forces immediately after full braking is initiated beginning from v_{max}, as at that moment the potential for force transfer is greatest due to the aerodynamic downforce. The greatest force occur at the front axis: vertically $F_{z2} = 2092\,\mathrm{N}$ and longitudinally $F_{x2} = 2299\,\mathrm{N}$. The camber angle is not affected by this loading, thus only a strength verification is necessary.
- **Load case 3: combined cornering and braking** An intermediate condition is modeled with approximately equal contributions from longitudinal and lateral forces (approaching a $45°$ angle in the Kamm circle [52]). Laboratory data, scaled appropriately, provide the resultant force magnitudes: $F_{z3} = 1200\,\mathrm{N}$ and longitudinally $F_{x3} = 2000\,\mathrm{N}$, and $F_{y3} = 1950\,\mathrm{N}$ laterally.
- **Load case 4: tire mounting** This case addresses the forces during tire installation, particularly the high internal pressure (often exceeding twice the operational pressure) applied to the rim, which can cause local overloading in the rim flange area. In this case, the maximum allowable tire pressure according the manufacturer is $p_{max} = 0.28\,\mathrm{MPa}$ is considered for a static strength evaluation.

- **Load case 5: Pothole impact at maximum speed** The vertical force during a pothole impact is simulated by assuming it – according to the recommendation of Trzesniowski [53] – as four times the static wheel load at v_{max}, ensuring that the rim can withstand the road bump load. The vertical load must be considered as $F_{z5} = 5672\,\mathrm{N}$ where the static strength requirement must be fulfilled.

The load cases must be evaluated differently depending on whether stiffness or strength is the governing criterion. The stiffness requirement based on the camber angle loss applies specifically to cornering. For the corresponding stiffness evaluation, load case 1A must be employed. Load case 3 also contains cornering, but the reduced lateral forces decrease the camber angle loss. Cornering load case 1B is deliberately not evaluated for stiffness because the camber angle limit is applicable only under competition conditions, while the scenario represented by load case 1B does not occur at a Formula Student event. Contrariwise, the strength evaluation must be performed for case 1B and all other load cases apart from 1A, since it applies proportionally higher forces than case 1A.

3.2 Finite element model building

The FE model of the rim must enable the evaluation of the strength and stiffness criteria while treating the composite laminate as an adaptable property.

Notably, the laminate sizing procedure must be formulated in a geometry-invariant manner to the outer rim contour which is fixed, due to the functional tire fitting requirement. The key feature to meet this fixed contour requirement is a surface model representing this outer contour with an inward stacking direction. The laminate stacking directions at the flanges and the beads must face inward, ensuring the model geometry remains independent of the laminate. The sketch in Fig. 7 shows the rim cross section with the respective stacking directions. However, according to this stacking, the rim offset is affected by the laminate thickness. Still, with the expected variation of the laminate thickness comprising only few millimeter, this influence is considered acceptable.

Aggarwal and Elsen [27] presented an iterative approach, in which the stacking sequence was adapted step-by-step to achieve an optimal laminate design. During the iterative design process, the rim laminates shall be adjusted and expanded until the previously defined stiffness and strength requirements are met.

To define the fiber orientation of each individual ply in the FE model, a cylindrical coordinate system is suitable, due to the axial symmetric geometry of the rim. The origin is located at the center of the rim which is also the origin of the global coordinate system. The $0°$ direction of the to the radial direction of the cylindrical system. Accordingly, the $90°$ direction represents the circumferential direction.

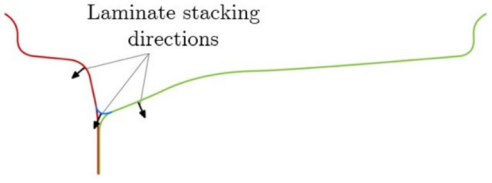

Fig. 7 Stacking directions for the composite sections of the shell elements representing the rim contour

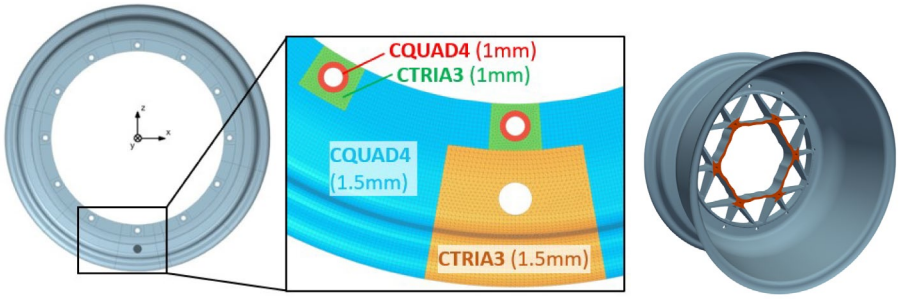

Fig. 8 FE shell mesh (**a**), element types, (**a**) and boundary conditions (**b**) for the hybrid rim FE model with the center disk

Table 3 Mesh convergence analysis for three different mesh densities

	Mesh 1	Mesh 2	Mesh 3
Element lengths	4 mm, 3 mm	2.5 mm, 2 mm	1.5 mm, 1 mm
Total elements N	24,880	53,925	155,808
Computation time	48 s	115 s	469 s
Maximum y displacements	9.36 mm	10.02 mm	10.06 mm

3.2.1 Discretization and model boundaries

For an accurate representation of local stress and deformation behavior, the discretization of the FE model and the choice of model boundaries are critical. Local stress hot spots may occur near features such as the bore holes for center disk mounting or the valve hole, so these must be included in the discretized model. The center disk's role was assessed through comparing the displacement results of two models with different model boundaries: first, a rim was clamped at the bore holes connecting to the center disk. Second, a rim model including the center disk was clamped at the disk's wheel hub interface as shown in Fig. 8b. This comparison revealed displacement increased by 17% for the model including the disk, which is considered crucial to the performance requirement. As a consequence, the disk must be part of the FE model.

The discretized FE model created in the simulation tool Siemens NX is depicted in Fig. 8a. Quadrilateral shell elements (CQUAD4) with six degrees of freedom per node were used wherever possible; only in transition zones triangular elements (CTRIA3) were required to maintain a regular mesh in areas predominantly meshed with CQUAD4. The CFRP laminate was modeled as a composite section using the ply properties in Table 4, while the aluminum center disk was modeled as isotropic. The aluminum center disk, due to its thickness, was modeled with CTETRA four-sided solid elements, as a compromise between accuracy and computational cost and meshing effort. In test runs with refined meshes the displacement differences were small compared with other modeling uncertainties. The CFRP shell rim is tied to the solid aluminum disk via displacement-compatible tie constraints at the bolted interface.

In the mesh convergence study, three FEM simulations were performed with progressively refined meshes according to Table 3. This process shall validate element sizes and ensure that further refinement would not yield significantly improved results but would only increase computational cost. The refinement rate, maintained as constant and calculated from the element counts N_i is given by Eq. (1).

$$r = \left(\frac{N_{i+1}}{N_i} \right)^{\frac{1}{3}} > 1.3 \tag{1}$$

This procedure ensures a systematic decrease in element size. Convergence was assessed using the nodal displacement in the y-direction under load case 1A. The Richardson extrapolation was employed to estimate a convergence limit and the Grid-Convergence-Index (GCI) was used to quantify convergence behavior. The results indicated that the finest mesh closely approximates the convergence limit (with a GCI of 1.003) confirming the adequacy of the mesh for subsequent analyses. Given the affordable computational costs shown in Table 3, the finest mesh can be employed for the design simulations.

3.2.2 Load introduction

According to the described load cases, the rim is loaded with vehicle forces and tire inflation pressure. The tire pressure directly applies to the entire rim's outer surface. Applying the vehicle load is more complex, as it is transmitted to the road through the tire. However, since tire modeling is inherently complex and introduces significant uncertainties, the load introduction is idealized by applying the tire forces F_x, F_y, F_z to a defined circumferential area of the rim bead seat. As depicted in Fig. 9, three circumferential sections — $15\,\%$, 25%, and 35% — were considered to assess the influence of this idealization.

Test simulations of load case 1A revealed, that the influence of the load introduction is relevant. However, due to prior experience of the Formula Student team, a load introduction on $25\,\%$ of the circumference is a plausible approximation that meets experimental reference results. Therefore, the design simulations are conducted with this variant. However, the uncertainty must be considered in the margin of safety for the strength evaluation.

3.3 Performance metric: camber angle loss

The stiffness requirement to the rim is formulated through a maximum camber angle loss of $0.2°\mathrm{g}^{-1}$ during the cornering load case 1A, with a maximum lateral acceleration of $2.3\mathrm{g}$. Hence, the permissible camber angle loss γ_{lim} for load case 1A is determined as $0.46°$ according to Eq. (2). This requirement directly applies to the wheel, as suspension

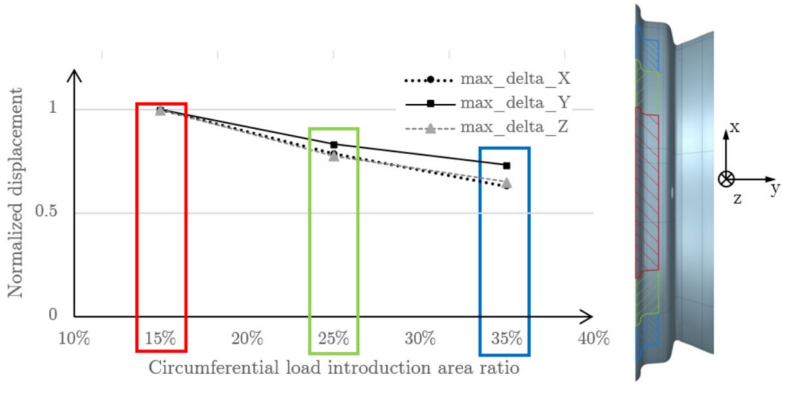

Fig. 9 Comparison of the normalized displacement for a varying tire load introduction area through circumferential sections of 15% (red), 25% (green), 35% (blue)

kinematics are evaluated independently, so the stiffness results are not affected by variations in suspension movement within this work.

$$\gamma_{lim} = 2.3\mathrm{g}\frac{0.2^\circ}{\mathrm{g}} = 0.46^\circ \tag{2}$$

The camber angle must be derived from the simulation result using the geometric relationship shown in Fig. 10 as the FE analysis does not directly provide the camber angle. Considering the rim radius $r_{rim} = 186\,\mathrm{mm}$ and the maximum camber angle loss, the permissible displacement in the *y*-direction at the rim's outer edge, y_{lim} is calculated as given in Equation (3).

$$\Delta y_{lim} = r_{rim} \cdot \tan(\gamma_{lim}) = 186\,\mathrm{mm} \cdot \tan(0.46^\circ) = 1.49\,\mathrm{mm} \tag{3}$$

The displacement in the *y*-direction for all nodes can be directly obtained from the FEM simulation. Under lateral load as in the case 1A, the rim deforms as shown in Fig. 10. As a result a positive displacement occurs at the rim periphery and a negative displacement in the center. The displacement of interest is the sum of these two contributions, representing the angular change relative to the original geometry.

3.4 Strength evaluation and safety factors

To design the laminate based on a quasi-static simulation, additional safety factors have to be considered to provide a reliable evaluation that accounts for fatigue, temperature, and uncertainty effects.

Due to the absence of a manufacturer-provided S-N curve for the anisotropic material and the infeasibility of conducting the necessary material tests with available resources, a fatigue safety factor of $S_{fatigue} = 2$ is employed according to Zanchini et al. [39], who also presented a design for a carbon fiber rim for a formula student car. This safety factor is applied to reduce the allowable stress for subsequent dimensioning and ensuring long-term durability.

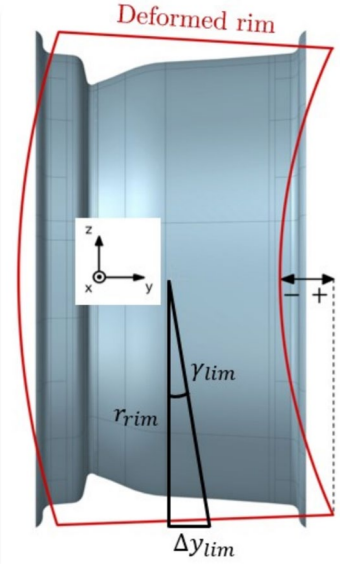

Fig. 10 Geometric derivation of the camber angle loss by the deformed rim and lateral load

The second safety factor accounts for the temperature-dependent behavior of the material. An analysis of the thermomechanical performance of fiber-epoxy composites indicates that at $100\,^{\circ}\mathrm{C}$, both stiffness and strength decrease by up to $10\,\%$. This temperature value is based on the team's experience regarding the expected conditions on the inner side of the rim which is exposed to the heat generated by the brakes. Accordingly, a temperature safety factor $S_{temp} = 1.11$ is applied.

The previously explained load introduction uncertainty also must be considered by a safety factor. The preliminary simulations indicate an expected fluctuation of up to $20\,\%$ in the *y*-direction depending on the load introduction. Consequently, the corresponding safety factor for the force introduction, $S_{loadintro} = 1.25$, is applied.

Normally, it is preferable to determine the actual material properties of a composite through a material characterization. However, as this is not feasible within the context of this work, the manufacturer's data is used and augmented with a safety factor. The datasheet for the material already specifies a potential deviation in strength and stiffness of $15\,\%$ [51], which leads to a material properties safety factor of $S_{data} = 1.18$.

All these factors must be multiplied to obtain the applicable safety factor $S_{strength}$ (Eq. (4)) for the strength assessment. The safety factor for strength is applied by dividing the material strengths from in Table 4 through the value of 3.27. Accordingly, the allowable stresses for tension in the 0° and the 90° direction, compression, and shear are $274\,\mathrm{MPa}$, $261\,\mathrm{MPa}$, $236\,\mathrm{MPa}$, and $27\,\mathrm{MPa}$ respectively, according to the strength parameters from Table 4 divided through the safety factor $S_{strength}$.

A safety factor $S_{stiffness}$ for the stiffness evaluation angle must only incorportate the values S_{temp}, $S_{loadintro}$, and S_{data} according to Eq. (5). Applied the permitted displacement calculated through Eq. (3), the safety factor reduces this value to a permitted displacement of $\Delta\tilde{y}_{lim} = 0.91\,\mathrm{mm}$.

$$S_{strength} = S_{stiffness} \cdot S_{fatigue} = 3.27 \tag{4}$$

$$S_{stiffness} = S_{temp} \cdot S_{loadintro} \cdot S_{data} = 1.64 \tag{5}$$

Table 4 Material data used for the FE analysis for the Cycom ® 985 prepreg as provided in the data sheet by Solvay [51] and for the 7022 aluminum alloy of the rim center disk

	Cycom ® 985 prepreg
E_{11t}	$65.4\,\mathrm{GPa}$
E_{22t}	$63.9\,\mathrm{GPa}$
E_{11c},E_{22c}	$57.9\,\mathrm{GPa}$
G_{12}	$4.6\,\mathrm{GPa}$
X_{11t}	$896\,\mathrm{MPa}$
X_{22t}	$855\,\mathrm{MPa}$
X_{11c},X_{22c}	$772\,\mathrm{MPa}$
X_{12}	$87.8\,\mathrm{MPa}$
ν_{12}	0.69
t_{ply}	$0.38\,\mathrm{mm}$
ρ	$1580\,\mathrm{kg/m^3}$
	Center disk aluminum
E	$72\,\mathrm{GPa}$
ν	0.33
ρ	$2760\,\mathrm{kg/m^3}$

For the laminate strength assessment the linear-elastic, orthotropic material model is used together with a ply-wise maximum-stress failure criterion. The maximum stresses are obtained from the datasheet strengths values in Table 4, divided by the strength safety factor $S_{\mathrm{strength}} = 3.27$. A ply is considered safe if all corresponding stress components remain below these reduced strengths.

The present analysis is restricted to quasi-static load cases composed from vehicle forces. Explicit 90°/13° impact tests, bending or fatigue tests and modal analyses of the wheel–suspension system (as required for road-legal rims), are not performed here. Their effects are partly covered by the conservative strength safety factor, but a full durability and impact validation is left to future work and would be required for road-worthy applications.

4 Results: laminate design and structural verification

4.1 Resulting laminate configuration

The laminate stacking was determined through an FE-based iterative sizing procedure, rather than employing a formal mathematical optimizer. The number and distribution of 0° and 45° plies were treated as discrete design variables, while the camber-angle-based stiffness limit and the stress constraints defined the admissible design space. Starting from an initial laminate, additional plies were added symmetrically and the stacking sequence was adjusted in discrete steps. After each update, the FE analysis was repeated until all stiffness and strength constraints were satisfied with minimal rim mass within the chosen ply-angle set. The sizing procedure was terminated once all stiffness and strength constraints were met with the lowest achievable rim mass (least number of plies) within the given discrete design space.

To determine how 0° and 45° fiber orientations influence the structural response, an initial comparison was performed for load case 1A. In a first simulation, only 0° plies were used. In the second, the fiber orientation was uniformly changed to 45° for the same number of plies. The results revealed, that the displacement with 0° plies is more than 50% lower than with 45° plies, demonstrating that 0° plies provide higher stiffness under the given load condition.

The key design variable to be determined was the number of plies. By iteratively adding additional plies, the stiffness of the rim was gradually increased. The sizing process is considered complete once the y-displacement limit of $0.91\,\mathrm{mm}$ load case 1A is achieved.

The initial analyses with pure 45° and 0° layups served as the base configuration for the iterative process shown in Fig. 11. It was observed that the $[0, 0, 0]_s$ layup resulted in a maximum lateral rim displacement Δy (cf. Fig. 10) is $2.2\,\mathrm{mm}$ while the layup $[45, 45, 45]_s$ entailed a displacement of $4.6\,\mathrm{mm}$, indicating that a significantly greater number of plies is required. As a consequence, two 0° plies were added symmetrically to the $0\,^\circ$ layup. The desired stiffness was achieved with a stacking sequence of ten 0° plies.

Further laminate modification was required to meet the design guidelines for fiber-reinforced composites [54, 55]. In particular, thick blocks of layers with identical fiber orientations should be avoided to maintain fatigue strength. Four inner plies were reoriented to 45° while retaining 0° plies on the outer surfaces to maximize stiffness, which resulted in the alternating sequence of $[0, 45, 0, 45, 0]_s$.

However, since the 45° plies provide lower stiffness than the 0° plies, this adjustment again led to an excessive maximum displacement in the y-direction. To maintain

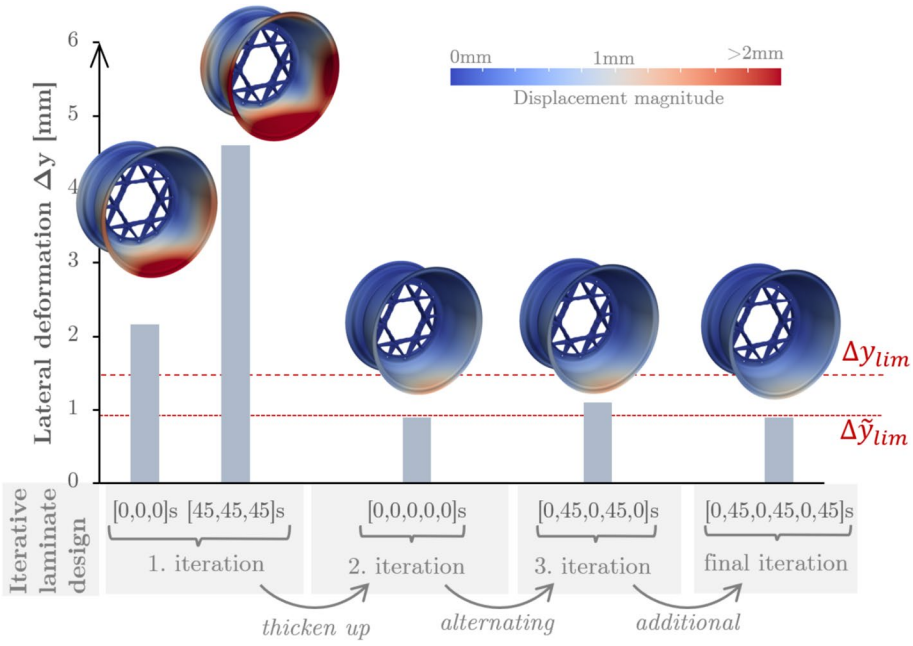

Fig. 11 Lateral rim displacement Δy for the iteratively adjusted laminates under load case 1A

symmetry in the laminate, two $45°$ plies were added in the middle, yielding a final stacking sequence of $[0, 45, 0, 45, 0, 45]_S$. With this twelve-ply symmetric configuration, the predicted displacement in the y-direction for load case 1A was $\Delta y = 0.904\,\mathrm{mm}$ meeting the displacement requirement and the laminate stacking rules.

The CFRP rim with the final stacking sequence has a mass of $m_{hybridrim} = 1.14\,\mathrm{kg}$. Including the aluminum center disk $m_{disk} = 0.65\,\mathrm{kg}$, the new rim has a total mass of $m_{rimtotal} = 1.79\,\mathrm{kg}$. In comparison to the conventional aluminum rim with the same center disk design, this is a weight reduction of 49%. This total mass and the weight reduction align well with the values reported in the literature for 13" rims of FS cars (cf. Fig. 2).

The aluminum rim serves as a mass reference, as no calibrated FE model of the original wheel is available for a one-to-one structural comparison. Even with this limitation, the mass reduction achieved by the hybrid CFRP rim remains the relevant indicator of the lightweight benefit: the design is intended to meet, rather than deliberately exceed, the defined stiffness and strength requirements, so further performance increase is not a design objective, whereas the achieved mass saving directly reflects the lightweight gain.

4.2 Individual load case results

The results for the final laminate configuration are summarized in Table 5 for all six load cases. As expected, the cornering scenario at maximum velocity produced the highest lateral displacements . The associated stress analysis confirmed that the cornering load case with v_{max} also generated the largest stresses for compression, tension, and shear. Peak stresses of $\sigma_{min} = -130\,\mathrm{MPa}$ and $\sigma_{max} = 171\,\mathrm{MPa}$ were observed, leaving safety factors of 1.5 for compression and 1.8 for tension. This indicates sufficient safety margins against strength or fatigue failure.

Regarding the other load cases, the higher pressure for the tire mounting (case 4) did not cause any critical stress levels. Braking loads from case 2 produced significantly

Table 5 Result plots of displacement magnitude, y-direction displacement and stress for all considered load cases. (The visualization was realized through Paraview [56])

	displacement magnitude	y-displacement	Stress[1]
Load Case 1A Cornering (competition)	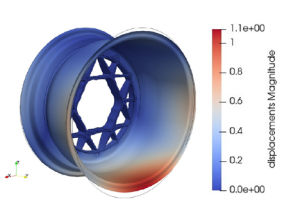	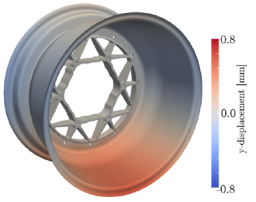	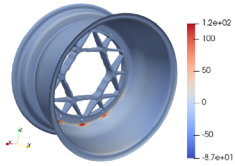 $\sigma_{min} = -95\,\text{MPa}$ $\sigma_{max} = 124\,\text{MPa}$ $\tau_{xy_{max}} = 7\,\text{MPa}$
Load Case 1B Cornering v_{max}	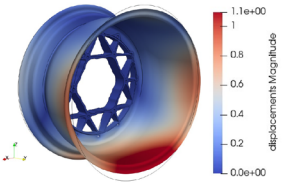	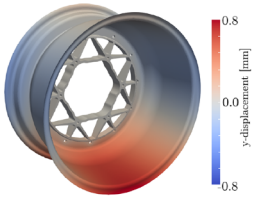	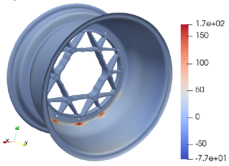 $\sigma_{min} = -130\,\text{MPa}$ $\sigma_{max} = 171\,\text{MPa}$ $\tau_{xy_{max}} = 9\,\text{MPa}$
Load Case 2 Full braking	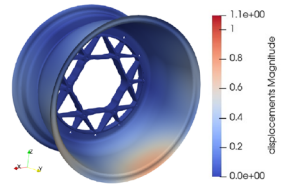	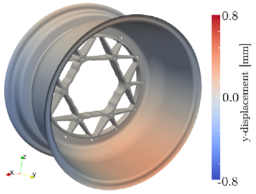	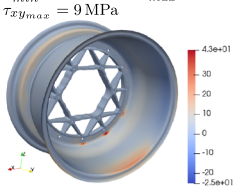 $\sigma_{min} = -74\,\text{MPa}$ $\sigma_{max} = 43\,\text{MPa}$ $\tau_{xy_{max}} = 4.4\,\text{MPa}$
Load Case 3 Combined	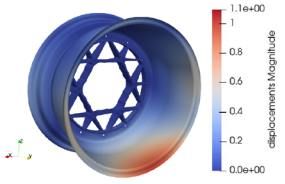	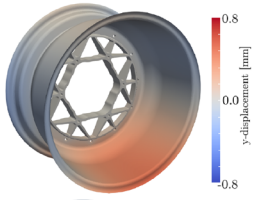	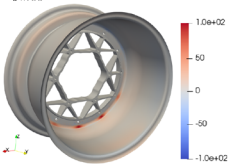 $\sigma_{min} = -103\,\text{MPa}$ $\sigma_{max} = 104\,\text{MPa}$ $\tau_{xy_{max}} = 6\,\text{MPa}$
Load Case 4 Tire mounting	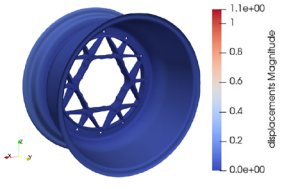	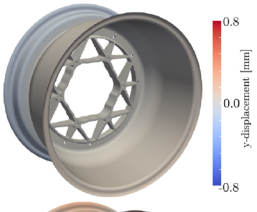	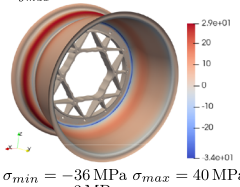 $\sigma_{min} = -36\,\text{MPa}$ $\sigma_{max} = 40\,\text{MPa}$ $\tau_{xy_{max}} = 3\,\text{MPa}$
Load Case 5 Pothole impact	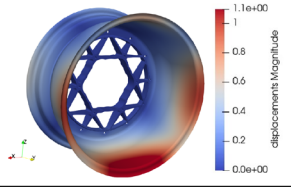	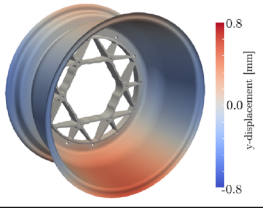	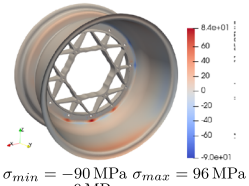 $\sigma_{min} = -90\,\text{MPa}$ $\sigma_{max} = 96\,\text{MPa}$ $\tau_{xy_{max}} = 9\,\text{MPa}$

[1] Stresses are plotted for the highest loaded ply.
The given stress values represent the extreme values of all plies.

lower stresses compared to cornering, while the combined loading case showed moderate stresses, quantitatively between braking and cornering. Although the pothole impact resulted in the largest radial displacements , the stresses associated with that high radial load remained lower than those from cornering. These results for all load cases confirm the robustness of the chosen laminate design.

Examining the stress distribution over the rim geometry, different hot spots can be observed. The highest stresses for nearly every load case occur near the valve hole in the outermost or innermost layers of the laminate stack. Further hot spots are the drop base and the screw holes for mounting the rim to the center disk.

4.3 Result validation through an enhanced FE model

To strengthen confidence in the analysis results and to prepare the design for manufacturing, an enhanced FE model was developed as part of the validation stage. While the preliminary model suited the iterative laminate optimization, the enhanced model incorporates the actual laminate stacking and local fiber orientations resulting from ply draping. This approach provides a more realistic representation of the manufactured rim and allows direct transfer of the ply definition into the production process.

Similar to the preliminary design model, this simulation is prepared by meshing the surfaces and implementing loads and boundary conditions. The primary improvement over the preliminary model lies in the construction of a surface model representing the actual composite plies. As Fig. 12a shows, the laminate plies were laid up in three distinct sublaminates. First, one sublaminate, [0, 45, 0, 45, 0, 45], was laid up on each part of the two-piece tooling. In the FE model, these sublaminates are represented by the two tooling faces (red and blue in Fig. 12a) and are assigned an outward stacking direction.

A third sublaminate with an inward stacking was introduced to represent the face sheet for the outer contour (blue face in Fig. 12a). This sublaminate had an inverted stacking sequence, [45, 0, 45, 0, 45, 0]. The adjacent sublaminates were tied together, creating the full, symmetric stacking sequence in each part of the rim. The uncertain laminate thickness did not allow us using this improved modelling approach for the design, as the shape of the base laminate faces and the relative position of the face sheet depend on the stacking.

In addition, the validation model accounts for the local fiber orientation resulting from the draping of the layer segments. As draping the individual plies in one piece would induce significant wrinkling, the plies are segmented into drapeable ply cuts. These cuts are obtained from a draping simulation using the Fibersim add-on in Siemens NX, as illustrated in Fig. 12b. The stacking now incorporates the ply cuts along with their realistic local fiber orientations. The individual ply segmentation was rotated about the rim's

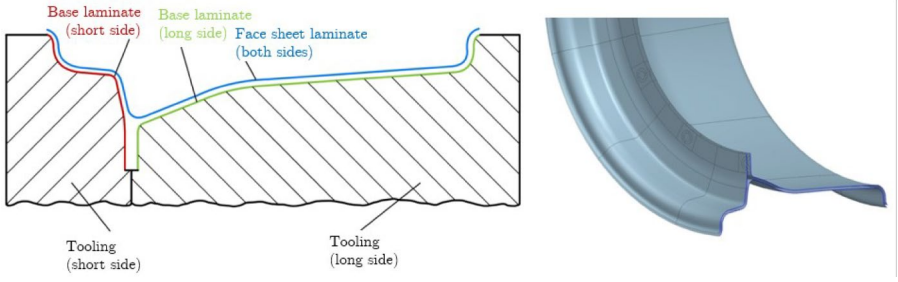

(a) Validation model based on three surfaces representing the sublaminates as in the manufacturable rim.

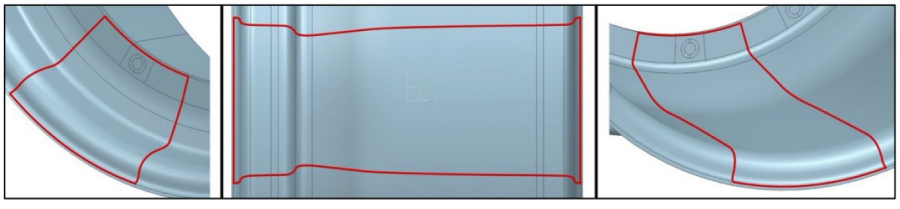

(b) Three examples for manufacturable ply segments.

Fig. 12 Features of the validation FE model

central axis for each ply, allowing for an extensive overlap between the adjacent layers. The seam position in the laminate was assigned layer by layer to the respective edges to achieve the most effective distribution of the weak spots.

The tooling geometry derived from the inner rim geometry, as shown in Fig. 12a, ca serve as the foundation for manufacturing. The cuts obtained from the ply segmentation according to Fig. 12b, can be used in the actual manufacturing process, guiding the placement of prepreg material onto the two-piece tooling. Hence, the validation simulation delivers the required preparations for the rim manufacturing process.

The load case 1A was applied to evaluate the enhanced model's stiffness. The calculated lateral displacement in the y-direction must not exceed the target value $\Delta\tilde{y}_{lim}$. According to the result given in Equation (6), this requirement is fulfilled. In addition, load case 1B, simulating cornering at maximum speed, was used for strength assessment.

The simulation results for the load case 1A are contrasted in Fig. 13. While the deformation was qualitatively consistent for both methods, notably, the displacement magnitude obtained from the validation model was nearly $20\,\%$ below the value calculated through the preliminary model, as Eq. (6) reveals.

$$\Delta y_{validation} = 0.74\,\mathrm{mm} < \Delta\tilde{y}_{lim} = 0.91\,\mathrm{mm} \tag{6}$$

The stiffness increase was attributed to two factors: First, the validation model neglects the screw holes in the flange area and the bore hole for the valve. To quantify the stiffening influence of these holes, an additional simulation was performed using the preliminary model with filled holes. A 5% displacement reduction was observed, which effectively translates into an equivalent increase in stiffness for the validation model. Second, a simplification in the preliminary model reduces the local stiffness: the small face at the drop bead (blue in Fig. 7) was bonded on small contact areas, causing a non-physical local deformation increase. In contrast, the validation model employs contact surfaces that follow the actual transitional areas, contributing positively to the overall stiffness of the structure. Consequently, the result of the validation model was considered more reliable, affirming the conservativeness of the rim design.

5 Discussion

5.1 Comparison with existing work

The final laminate configuration meets the main design targets for the composite rim. The camber-angle-based performance criterion is satisfied with a lateral displacement of $\Delta y = 0.904\,\mathrm{mm}$ under the critical cornering load case, just below the limit of $\Delta\tilde{y} = 0.91\,\mathrm{mm}$.

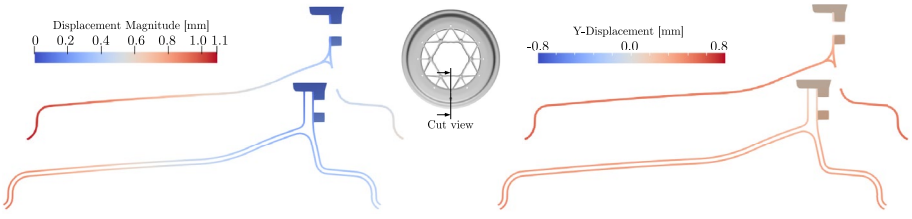

Fig. 13 Displacement magnitude (left) and y-displacement (right) results of the validation model compared to the preliminary design model for the load case 1A

A full FE re-analysis of the aluminum rim was not available within the project scope; therefore, the comparison to the baseline focuses on mass and on meeting identical stiffness and strength requirements under the same load cases, rather than on a detailed stress–strain comparison between the two geometries.

At the same time, all relevant stress components remain within conservative allowables, with safety factors of about 1.5 in compression and 1.8 in tension. The hybrid rim mass of $1.79\,\mathrm{kg}$ (including the aluminum center disk) corresponds to a 49% reduction compared to the reference aluminum rim and a decrease of roughly 3% in total vehicle mass. For a FS car, this reduction in unsprung and rotating mass is expected to improve handling and efficiency as outlined in the literature [12, 29].

In the context of other CFRP rims for Formula Student and FS vehicles, the present design lies in the upper range of reported mass savings (cf. Fig. 2). Compared to full-composite rims, hybrid concepts with metallic center disks generally offer slightly lower mass savings but simpler manufacturing and hub integration [27, 31]. The 49% reduction achieved here compares favorably to these hybrid solutions and approaches the lightweight performance of some full composite rims, while remaining compatible with the existing hub and the resources of a student team.

Several previous studies propose iterative or optimization-based workflows for composite wheels. Barsony et al. [33] describe a manual layup iteration for an FS rim. However, recent automotive design work explores surrogate-based multi-objective optimization for composite rims [40] and impact/ fatigue assessment [39, 41]. These approaches demonstrate the potential of formal optimization and extensive testing, and outline the future work steps to be accomplished to for a further design improvement. In contrast to surrogate-based multi-objective optimization frameworks for CFRP rims, the present work deliberately adopts a low-overhead, manually guided sizing strategy that can be implemented within the limited resources of a student team.

The present study offers an FE-based laminate sizing methodology that is intentionally simple and geometry-invariant. The outer contour is fixed by the tire specification, and the laminate is parameterized through discrete ply counts and orientations that are iteratively adjusted to satisfy stiffness and strength constraints.

An enhanced FE model with realistic ply draping links this abstract laminate definition to a manufacturable layup. The rim has not been tested yet and that all results are based on FE simulations. Within the limits of the chosen ply set and the absence of experimental validation, the study shows how a transparent, transferable design workflow for CFRP rims can be implemented under the practical constraints of an FS project and how its outcome compares with existing FS and automotive progress.

Crash load cases, modal behavior, and environmental degradation are not considered in the present analysis and should be addressed in future work, especially for applications beyond the controlled Formula Student environment (Table 6).

5.2 Alternative laminate configurations

The achieved stacking pattern in the presented design was derived on the assumption that the laminate must be build from woven plies of the two orientations $0°/90°$ and $\pm 45°$. Constraints from manufacturing feasibility and material availability in the Formula Student context imposed this requirement in the present study. Nonetheless,

Table 6 Summary of main design objectives and corresponding outcomes for the hybrid CFRP rim

Design objective	Outcome
Reduce rim mass compared to aluminum reference	Rim mass reduced by 49% (3.53 kg → 1.79 kg including center disk), leading to an overall vehicle mass reduction of about 3%
Meet camber-angle limit under critical cornering load	Lateral displacement $\Delta y = 0.904\,\mathrm{mm}$ for load case 1A, below the allowable $\Delta\tilde{y} = 0.91\,\mathrm{mm}$
Satisfy strength constraints under all relevant load cases	Maximum ply stresses within allowable limits; safety factors of approximately 1.5 in compression and 1.8 in tension for the most critical regions
Ensure manufacturability and integration with existing vehicle	Layup compatible with prepreg processing in a two-piece tool; practical ply cuts and draping strategy defined; rim geometry and interfaces remain compatible with the existing hub and center disk

suitable stackings can also be derived also for different laminate families while keeping the same sizing workflow.

If unidirectional plies are available to tailor the stacking, an elementary variation is the classical legacy quad stacking, composed of the orientations $0°, 90°$ and $\pm 45°$ [57]. A quad laminate features a controllable number of plies for each of these orientations, which is favourable to optimize stacking. For example, the optimized design by Walther [13] features a higher ply share in the circumferential $0°$ direction, while the optimum found by Unti et al. [30] has a higher $90°$ ply share. Moreover, legacy quad laminates offer a good damage tolerance against accidental damage, due to many ply interfaces in the layup.

Alternatively, the double-double laminate family ($[\pm\phi, \pm\psi]_n$) [58, 59] could be employed to design the rim laminate. The design variables become the ply angles and the number of plies for each orientation, while the constraints (first of all the camber-angle limit, but also stress allowables and manufacturability) are evaluated. Local tailoring can further be introduced by separately designing the laminate on both half-sides of the rim

5.3 Current limitations

The analysis in this study is limited to quasi-static load cases derived from Formula Student regulations and typical racing operation. Dynamic loads, detailed fatigue investigations with spectrum loading, and impact or even crash scenarios are explicitly included. The considered knock down factors accounting for these effects introduce a certain safety against failure, however they do not reflect the behaviour of individual laminates under these conditions. Moreover, the current design has not been validated experimentally, as no prototype rim was available at this stage. Future work will therefore focus on manufacturing a prototype, instrumented stiffness and strength tests, and dedicated fatigue and impact investigations to validate and, if necessary, refine the numerical model.

6 Conclusion and outlook

This work presented the development of a production-ready lightweight composite rim for a Formula Student race car. Based on a literature survey of existing CFRP rim concepts for FS and related automotive applications, a hybrid solution with a CFRP rim and aluminum center disk was selected and sized using an FE-based laminate design process. The resulting rim meets the stiffness (performance) and strength requirements under representative racing load cases and achieves a 49% mass reduction compared to the conventional aluminum rim, corresponding to an overall vehicle mass reduction of about 3%.

Beyond the specific rim geometry, the main contribution of this study is the design methodology itself. The FE analysis is embedded in a workflow that enables geometry-invariant laminate sizing: the laminate is parameterized by discrete ply counts and orientations and iteratively adapted within clearly defined load cases, performance criteria, and strength limits. Because the sizing is formulated with respect to these constraints rather than a single fixed geometry, the same procedure can be transferred to other wheel concepts or sizes, for example to full-composite spoke rims or 10 inch rims.

Future work will focus on manufacturing a prototype rim and experimentally validating the numerical predictions for stiffness and strength. In addition, the damage tolerance and fatigue behavior of the design should be investigated in more detail, including impact-related load cases and durability considerations similar to those applied to roadworthy rims. These steps would further substantiate the methodology and support its application in broader lightweight wheel design studies.

Appendix

Definitions and nomenclature of the rim components

The geometric definitions of a rim and its components are shown in Fig. 14. Position 1 shows the rim flanges, which, together with the tire's internal pressure, prevent the tire from slipping outward and ensure tightness. Due to high loads, the flanges must be very rigid. To prevent tire slipping toward the center, the rim humps (position 2) are circumferential elevations that securely position the tire. The hump also takes lateral forces under high load during cornering. Modern designs typically feature a hump on both sides of the rim. Position 3 indicates the rim bead seat, where the tire bead (the edge of the tire) sits between the flange and the hump. The internal tire pressure also acts on this area. The rim diameter (position 5) is measured at the bead seat (10" or 13" for the rim sizes relevant to the FS). The rim width (position 6) is represented by the distance of both bead seats. The two rim bead seats are joined by a drop center (position 4). This drop center enables tire mounting for one-piece rims. (In contrast, flat-bed rims require a two-part design to

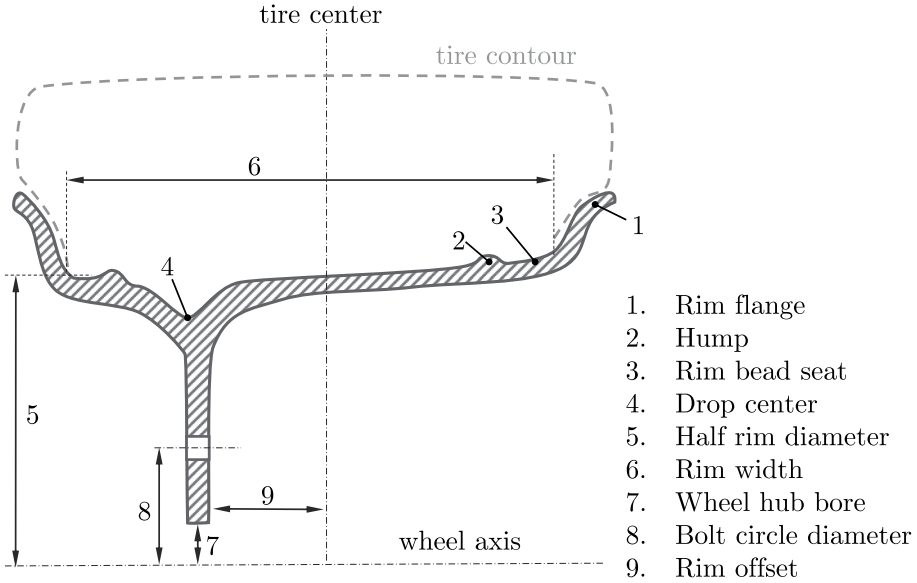

Fig. 14 Cut view of a half rim to outline the design-relevant rim features according to the standard [47].

mount the tire, which increases the complexity.) The rim center continues toward the bolt circle (position 8) and a central bore (position 7) where the rim is attached to the wheel hub. (In case of a multi-piece rim with a separate center disk, the bolt circle for the dis attachment is located directly below the drop center and the disk closes the gap between the rim and the wheel hub.) The geometry metrics. The rim offset (position 9) is the measured distance from the rim mounting surface to the centre line of the wheel.

Acknowledgements
The authors gratefully acknowledge the support and contributions of the Lions Racing Team Braunschweig, the German Aerospace Center (DLR), and the Institute for Engineering Design at the Technische Universität Braunschweig, and by Siemens Digital Industries Software for sponsoring the Siemens NX software license.

Author contributions
K.K. and R.B. wrote the main manuscript text and prepared the Figures. K.K. contributed to conceptualization, methodology, validation, formal analysis, investigation, data curation. R.B. contributed to conceptualization, validation, formal analysis, investigation and supervised the project. J.L. performed the simulation tasks and contributed to conceptualization, investigation, formal analysis, data curation, writing – review & editing, and supervision. L.T. researched design and industry standards, contributed to investigation, writing – review & editing, and the project supervision. All authors reviewed the manuscript.

Funding
Open Access funding enabled and organized by Projekt DEAL. The authors declare that no fund has been received to support the presented research.

Data availability
The simulation and design data produced in this study are available from the corresponding author upon reasonable request.

Declarations

Ethics approval and consent to participate
Not applicable.

Consent to publish
Not applicable.

Competing interests
The authors declare no competing interests.

Received: 22 September 2025 / Accepted: 13 February 2026
Published online: 26 February 2026

References

1. FSG: Formula Student Rules 2025 V1.1. Formula Student Germany. 2025–03-19 (2025). https://www.formulastudent.de/fsg/rules/.
2. IMECH: History of Formula Student. Institution of Mechanical Engineers. 2025–03-19 (2025). https://www.imeche.org/events/formula-student/about-formula-student/history-of-formula-student.
3. FSG: Registered Teams Formula Student Germany 2025. Formula Student Germany. 2025–03-19 (2025). https://www.formulastudent.de/teams/registered/2025.
4. Mihailidis A, Samaras Z, Nerantzis I, Fontaras G, Karaoglanidis G. The design of a formula student race car: a case study. Proc Inst Mech Eng Part D J Automobile Eng. 2009;223(6):805–18. https://doi.org/10.1243/09544070JAUTO1080.
5. Yan L, Xu H. Lightweight composite materials in automotive engineering: State-of-the-art and future trends. Alex Eng J. 2025;118:1–10.
6. Zhang S, Song H, Xu L, Cai K. Application research on the lightweight design and optimization of carbon fiber reinforced polymers (cfrp) floor for automobile. Polymers. 2022;14(21):4768.
7. Li S, Wang D, Wang S, Zhou C. Structure-connection-performance integration lightweight optimisation design of multi-material automotive body skeleton. Struct Multidiscip Optim. 2023;66(9):198.
8. Li S, Wang D, Zhou C. Multi-level structural optimization of thin-walled sections in steel/aluminum vehicle body skeletons. Appl Math Model. 2024;132:187–210.
9. Li S, Zhou D, Pan A. Integrated lightweight optimization design of wall thickness, material, and performance of automobile body side structure. Struct Multidiscip Optim. 2024;67(6):95.
10. Sakundarini N, Taha Z, Abdul-Rashid SH, Ghazila RAR. Optimal multi-material selection for lightweight design of automotive body assembly incorporating recyclability. Mater Des. 2013;50:846–57.
11. Boria S. Lightweight design and crash analysis of composites. In: Lightweight Composite Structures in Transport, pp. 329–360. Elsevier, ??? 2016.
12. Hrovat D. Influence of unsprung weight on vehicle ride quality. J Sound Vib. 1988;124(3):497–516. https://doi.org/10.1016/S0022-460X(88)81391-9.

13. Walther HW. Development of a lightweight laminated composite wheel for formula sae race vehicles. PhD thesis, University of Kansas 2016. https://kuscholarworks.ku.edu/handle/1808/21984.
14. Sorrenti D, Smout C. Wheel design and development for the Formula Student 2020 Race Car of The University of Nottingham 2020. https://doi.org/10.13140/RG.2.2.20696.52484/1
15. Bhagwat PGG. Design and Analysis of A 10" Carbon Fiber Wheel for a Formula SAE Racecar. Mechanical and Aerospace Engineering Theses. 2017;912. https://mavmatrix.uta.edu/mechaerospace_theses/912.
16. Ślaski G, Gudra A, Borowicz A. Analysis of the influence of additional unsprung mass of in-wheel motors on the comfort and safety of a passenger car. Archiwum Motoryzacji 2014;65(3), 51–64. https://bibliotekanauki.pl/articles/1364140.pdf.
17. Wu P, Luo R, Yu Z, Hou Z. Evaluation of the unsprung mass effect on ride comfort of in-wheel motor driving vehicles. Proceedings of the Institution of Mechanical Engineers, Part D: Journal of Automobile Engineering 2004. https://doi.org/10.1177/09544070241288615
18. Luo Y, Tan D. Study on the dynamics of the in-wheel motor system. IEEE Trans Veh Technol. 2012;61(8):3510–8. https://doi.org/10.1109/TVT.2012.2207414.
19. Clarke P. Pat's Corner: Tyres. Formula Student Germany (FSG). https://www.formulastudent.de/pr/news/details/article/tyres [Accessed: 2025–08-27] 2006.
20. Orlando S. Transmission design for a formula student electric race car: Geartrain evolution for transition from 13" to 10" rims. PhD thesis, Politecnico di Torino (2023). https://webthesis.biblio.polito.it/29148/.
21. Korntved K, Hersbøll J, Lauritsen M, Bording K, Leto H. Design and Analysis of a Formula Student Carbon Fibre Rim. Aalborg University, Denmark: Department of Materials and Production 2017. https://www.aaudxp-cms.aau.dk/media/wimntaxu/design-and-analysis-of-a-formula-student-carbon-fibre-rim.pdf.
22. Daubach K, Gummel A, Kohns L, Kerscher E. Failure analysis on a fractured rim star of a formula student racing car. Pract Metallogr. 2016;53(2):98–111. https://doi.org/10.3139/147.110369.
23. Bol'shikh A, Vdovin D, Eremin G. Calculation investigation of the strength of the composite wheel rim. Izvestiya MGTU MAMI 2018;12(1), 2–9. https://doi.org/10.17816/2074-0530-66814
24. Keizer: Keizer Aluminum Wheels: FSAE. K2W Precision Inc. https://keizerwheels.com/product-category/fsae/ [Accessed: 2025–08-27].
25. OZ-Racing: Formula Student. OZ S.p.A. https://www.ozracing.com/motorsport/formula-student/wheels [Accessed: 2025–08-27].
26. Rohan CD. Design and analysis of a composite wheel rim. J Mat Sci Mech Eng. 2015;2(6):50–6.
27. Aggarwal S, Elsen R. Design and fabrication of cfrp wheel centre for fsae race-car. Technical report, SAE Technical Paper 2019. https://doi.org/10.4271/2019-28-0117
28. Czypionka S, Kienhöfer F. Weight reduction of a carbon fibre composite wheel. Sci Eng Compos Mater. 2019;26(1):338–46. https://doi.org/10.1515/secm-2019-0018.
29. Kandukuri SY, Pai A, Manikandan M. Scope of carbon fibre-reinforced polymer wheel rims for formula student racecars: A finite element analytical approach. Journal of The Institution of Engineers (India): Series C 2022;103(4), 939–948. https://doi.org/10.1007/s40032-022-00808-w
30. Unti EK, Shorab AZ, Kragen PB, Menashe AM. Reinventing the wheel 2018. https://digitalcommons.calpoly.edu/mesp/457/.
31. Uyttersprot B. Analysis of a carbon fibre rim: Student formula 2015.
32. Shekhar MC, Rao BL, Krishna M. Design and structural analysis of car alloy wheel using with various materials. International Journal of Advance Scientific Research and Engineering Trends 5 2020.
33. Bársony D, Kaszab M, Feszty D. An iterative method for the design of carbon-fiber reinforced polymer wheel rims. Appl Sci. 2025;15(21):11434.
34. Ressa A. Development of a carbon fiber wheel rim. PhD thesis, The Ohio State University 2013. https://kb.osu.edu/server/api/core/bitstreams/3a6ade6d-0285-5bb8-9c6f-8b698e132c5e/content.
35. Kruse P, Wathen HJ, Hyde JJ, Dobben ND, Blake JD. Design and analysis of one-piece 10" carbon fiber wheels for zips racing zr20 formula sae racecar 2021.
36. Pizot SL, Martin L, Warner J, Levis J. C6 wheels 2019.
37. Nishi M. Study of weight reduction and performance control by cfrp local modifying technology. SAE Technical Paper: Technical report; 2018.
38. Malewadkar D, Majumder H. Optimizing car wheel rim mass and design: A composite material approach with finite element analysis. Mater Eng Technol. 2025;1(1):39–51.
39. Zanchini M, Longhi D, Mantovani S, Puglisi F, Giacalone M. Fatigue and failure analysis of aluminium and composite automotive wheel rims: Experimental and numerical investigation. Eng Fail Anal. 2023;146:107064. https://doi.org/10.1016/j.engfailanal.2023.107064.
40. Wang D, Xu W, Wang Y, Gao J. Design and optimization of tapered carbon-fiber-reinforced polymer rim for carbon/aluminum assembled wheel. Polym Compos. 2021;42(1):253–70.
41. Hwang S-F, Yu H-L, Liu Y-J, Chen Y, Chen S-C, Hsieh Y-C. Progressive failure of metal-composite hybrid wheels under impact. J Mech Sci Technol. 2018;32(1):223–9.
42. Bisht PS, Awasthi A. Design and analysis of composite and al alloy wheel rim. In: Singh I, Bajpai PK, Panwar K, editors. Advances in Materials Engineering and Manufacturing Processes. Singapore: Springer; 2020. p. 15–29.
43. ISO14400: ISO 14400:2021: Road vehicles — Wheels and rims — Use, general maintenance and safety requirements and out-of-service conditions. Standard, International Organization for Standardization, Geneva, CH (October 2021).
44. ISO3006: ISO 3006:2015: Road vehicles — Passenger car wheels for road use — Test methods. Standard, International Organization for Standardization, Geneva, CH (June 2015).
45. Weymar E, Finkbeiner M. Statistical analysis of empirical lifetime mileage data for automotive lca. Int J Life Cycle Assess. 2016;21(2):215–23. https://doi.org/10.1007/s11367-015-1020-6.
46. Jimenez-Martinez M. Artificial neural networks for passive safety assessment. Engineering Letters 2022;30(1).
47. ISO3911: ISO 14400:2021: Wheels and rims for pneumatic tyres — Vocabulary, designation and marking. Standard, International Organization for Standardization, Geneva, CH (October 2021).
48. Ekermann T, Hallström S. Pull-off tests of cfrp t-joints with conventional and 3d reinforced fillets. Composite Structures 2019;223, 110893. https://doi.org/10.1016/j.compstruct.2019.110893

49. Bogenfeld R, Gorsky C, Wille T. An experimental damage tolerance investigation of cfrp composites on a substructural level. Composites Part C: Open Access 8, 100267 (2022) https://doi.org/10.1016/j.jcomc.2022.100267
50. Mohammed U, Lekakou C, Bader M. Experimental studies and analysis of the draping of woven fabrics. Compos A Appl Sci Manuf. 2000;31(12):1409–20. https://doi.org/10.1016/S1359-835X(00)00080-4.
51. Solvay SA. Technical Data Sheet: Cycom® 985 and Cycom® 985LV prepreg. 2017. Solvay SA.
52. Frömmig L. Racing tires. In: Basic Course in Race Car Technology: Introduction to the Interaction of Tires, Chassis, Aerodynamics, Differential Locks and Frame, pp. 59–88. Springer. 2023. https://doi.org/10.1007/978-3-658-38470-8
53. Trzesniowski M. Fahrwerk, pp. 245–390. Vieweg+Teubner, Wiesbaden 2010. https://doi.org/10.1007/978-3-8348-9667-4
54. Bogenfeld R, Freund S, Dähne S, Wunderlich T, Wille T. Damage tolerance allowable calculation for the aircraft design with static ultimate load. Composite Structures, 2023;117803. https://doi.org/10.1016/j.compstruct.2023.117803
55. Wang GD, Wang J, Hossain SKM, Chen H. Research on design rules for composite laminate. Sci Eng Compos Mater. 2015;22(3):315–23. https://doi.org/10.1515/secm-2013-0251.
56. Ayachit U, Geveci B, Moreland K, Patchett J, Ahrens J. The ParaView Visualization Application. 2012.
57. Kassapoglou C. Design and Analysis of Composite Structures: with Applications to Aerospace Structures. Wiley Online Library, ??? 2010.
58. Tsai SW. Double-double: new family of composite laminates. AIAA J. 2021;59(11):4293–305.
59. Kappel E. Double-double laminates for aerospace applications—finding best laminates for given load sets. Composites Part C Open Access. 2022;8:100244.

Publisher's Note